UC Irvine
UC Irvine Previously Published Works

Title

Spectral phasor analysis of LAURDAN fluorescence in live A549 lung cells to study the hydration and time evolution of intracellular lamellar body-like structures

Permalink

https://escholarship.org/uc/item/1c00b5gp

Journal

Biochimica et Biophysica Acta, 1858(11)

ISSN

0006-3002

Authors

Malacrida, Leonel
Astrada, Soledad
Briva, Arturo
et al.

Publication Date

2016-11-01

DOI

10.1016/j.bbamem.2016.07.017

Peer reviewed

Spectral Phasor analysis of LAURDAN fluorescence in live A549 lung cells to study the hydration and time evolution of intracellular lamellar body-like structures

Leonel Malacrida[a,b,c,*,1], **Soledad Astrada**[d,2], **Arturo Briva**[a], **Mariela Bollati-Fogolín**[d], **Enrico Gratton**[c], and **Luis A. Bagatolli**[e,*]

[a]Área de Investigación Respiratoria, Departamento de Fisiopatología, Hospital de Clínicas, Facultad de Medicina, Universidad de la República, Uruguay

[b]Unidad de Bioquímica y Proteómica Analítica, Institut Pasteur de Montevideo, Uruguay

[c]Laboratory for Fluorescence Dynamics, Biomedical Engineering Department, University of California at Irvine, Irvine, California-USA

[d]Unidad de Biología Celular, Institut Pasteur de Montevideo, Uruguay

[e]MEMPHYS - Center for Biomembrane Physics, University of Southern Denmark, Odense M, Denmark

Abstract

Using LAURDAN spectral imaging and spectral phasor analysis we concurrently studied the growth and hydration state of subcellular organelles (Lamellar Body-like, LB-like) from live A549 lung cancer cells at different post-confluence days. Our results reveal a time dependent two-step process governing the size and hydration of these intracellular LB-like structures. Specifically, a first step (days 1 to 7) is characterized by an increase in their size, followed by a second one (days 7 to 14) where the organelles display a decrease in their global hydration properties. Interestingly, our results also show that their hydration properties significantly differ from those observed in well-characterized artificial lamellar model membranes, challenging the notion that a pure lamellar membrane organization is present in these organelles at intracellular conditions. Finally, these LB-like structures show a significant increase in their hydration state upon secretion, suggesting a relevant role of entropy during this process.

[*]Corresponding author. lmalacrida@hc.edu.uy (L. Malacrida) or bagatolli@memphys.sdu.dk (L.A. Bagatolli).
[1]LM and SA contributed equally to this work.

Conflict of interest

The authors declare no competing financial interests.

Supporting Material

Additional data are available as supplementary information online

Graphical abstract
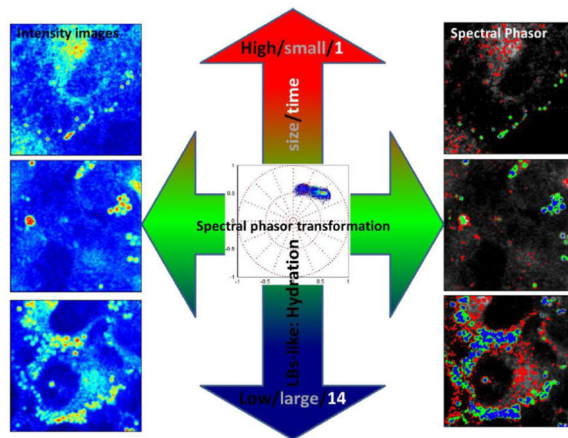
Keywords

LAURDAN; spectral phasor; Lamellar Bodies; membrane biophysics; microscopic imaging; macromolecular crowding

1. Introduction

The spectral phasor analysis appeared a few years ago as a useful method to unmix fluorescence spectral images obtained from multiple-labeled specimens with minimal input [1] or to analyze the complex fluorescence emission of the well-known LAURDAN properties to study membrane dynamics [2]. This type of analysis has emerged as a promising tool to disentangle relevant aspects of distinct membranous systems.

Currently, many aspects related to the organization and function of cellular membranes are topics of intense studies and controversy [3,4]. Specifically, the lack of understanding of relevant physical properties of intracellular membranes existing in cells is remarkable, particularly those that produce and accumulate lipids in subcellular organelles [5–7]. Examples of those kinds of systems are lamellar bodies from specialized lung cells.

Lamellar bodies (LBs) from lung pneumocyte type II cells (AT-II) are responsible for the storage of pulmonary surfactant (PS) at the cellular level. This organelle has been described as a lipid-rich proteolipid structure highly packed in concentrically organized multilamellar structures with a diameter of 1–3 μm [8]. PS comprises an important biological material during breathing since it allows the reduction of the surface tension in the lung's alveoli [9], essential to the mechanics of respiration.

The development of LBs is derived from the trans-Golgi pathway where this organelle initially grows as multivesicular bodies (MVB) [10]. In a later stage MVBs turn into composite bodies (CB; also known as immature LBs) and finally become mature organelles [10]. It has been reported that Surfactant protein B (SP-B) and ATP-binding cassette transporter A3 (ABCA3) are required for growth and maturation of LBs, which is an ATP-

consuming process [9]. However, there are still several open questions regarding the *in cellulo* organization and maturation of these highly specialized membranous intracellular structures.

It has been proposed that the extracellular secretion of LBs depends on physical and chemical signals, wherein stretch is mostly responsible for release of these organelles compared to synthetic exocytosis [11]. The molecular mechanism underlying exocytosis is a very specialized process that involves cytoskeletal machinery (F-Actin) [12] and particular proteins like Annexin 2 and 7 [13,14], SNAP-23 [15] and ABCA-3 [16]. As with many other secretory pathways, the LB secretory machinery uses Ca^{2+} as a second messenger [17]. Intracellular levels of Ca^{2+} are quite stable and a threshold of 320 nM is needed to trigger the release of LBs [18]. Several mechanisms are potentially involved in the initial calcium influx: mechanical stress, ATP release, phorbol ester and beta-adrenergic signaling [19]. However, three different populations of LBs have been described so far, one that is released rapidly after Ca^{2+} signaling (a few seconds after the calcium threshold is reached), a second one that is released within half an hour after Ca^{2+} signaling, and a third one (which represents >50% of the LBs) that does not respond to Ca^{2+} at all [20]. The reason for the lack of sensitivity to Ca^{2+} in this last population of LBs is unclear and is still a matter of investigation.

All these processes are highly regulated and, for example during exercise [21], the release of LBs is increased by the release of pre-attached organelles [22]. Upon secretion LBs are located in the epithelial lining fluid (a thin sheet of aqueous solution that covers the alveoli) and are subsequently transformed into a very complex structure called tubular myelin [20]. On the other hand, the mechanism for LBs adsorption into the air/water interphase has been carefully studied by Hobi *et al.* [23]. These authors described how temperature, ionic strength, pH and other relevant physicochemical factors modulate their adsorption at the alveolar interphase [23], also suggesting the occurrence of "solid-like" domains in the surfactant monolayer formed upon adsorption of LBs to the air/water interphase [24]. Additionally, in a recent study these authors report that intracellular LBs membranes from rat ATII cells exist as crystalline-like highly ordered structures, with a high packed and dehydrated state relative to the pulmonary surfactant isolated from lung lavages [25].

Classical transmission electron microscopy (TEM) has been the most popular tool to study the maturation process and structure of LBs. However, information obtained in live cells is precluded under these experimental conditions [26]. For instance, cell fixation protocols involve dehydration of the specimen in a series of acetone/Epoxy resins and low temperature [26], a process that impacts on the supramolecular organization of membranes. This problem can be also generalized to experiments performed using cryo-electron microscopy, wherein temperature and pressure are strongly modified (−196°C and 2000 bar pressure) [26] likely affecting membrane structure. Important effects of pressure impacting on membrane structure have been very documented in the literature [27].

With the advent of novel analytical tools associated with laser scanning confocal fluorescence microscopy, the problems mentioned above can be avoided; i.e. different methods are available to perform non-invasive studies of living specimens at different length

and time scales. As mentioned above, spatially resolved spectral data obtained using the fluorescent membrane probe 6-dodecanoyl-2-dimethylamino (LAURDAN) can be analyzed by the spectral phasor method [2]. This method is based on the Fourier transformation of the emission spectra of LAURDAN (that can be also used to analyze spectral information obtained from a fluorimeter [28]) and have been shown to be a powerful tool to analyze data from cellular and model membranes [2,28]. These Fourier transformations allow one to determine, with a simple visual inspection, the presence of complex interactions in the LAURDAN/membrane system without the assumption of a particular model as required by the classical Generalized Polarization function [28]. It is important to note, that the fluorescence emission of LAURDAN is extremely sensitive to the physical state of membranes, responding to the extent of water relaxation (hence the hydration state) occurring around the fluorophore moiety inserted in membranous structures [29,30].

The study reported here applies the experimental approach described in the preceding paragraph to correlate *in cellulo* time dependent size changes of LBs with their inherent hydration properties. It also attempts to study their hydration state before and after secretion, allowing for a detailed comparison with well-characterized suspensions of artificially produced lamellar model membranes using similar experimental methods. Albeit primary cell culture of pneumocyte type II has been extensively used to study LBs, these cells are difficult to culture for the long periods of time relevant in our studies (up to 14 days). Therefore we decided to use A549 cells, which belong to an immortalized cell line derived from a lung carcinomatous tissue as a cellular model. Although there are some contradictory results in the literature related to the composition of A549 Lamellar Body-like (LB-like) organelles [31,32], their presence in A549 cells was established by the regular TEM imaging or molecular markers like ABCA3 transporter or specific dyes [33–38]. These experimental evidences (some of them retested in our work, see results section) support the tenet that A549 cells synthesize and release LB-like organelles in culture. To avoid confusions and acknowledge the fact that we are using a model cell system (A549 cells), we decided to use the term LB-like structures instead of merely LB.

2. Material and Methods

2.1. Chemicals

Lipids were purchased from Avanti Polar Lipids (Alabaster, AL). 6-dodecanoyl-2-dimethylaminonaphthalene (LAURDAN) was acquired from Molecular Probes - Life Technologies (Thermo Fisher Scientific Inc.). All chemicals and supplies used for cell culture were purchased from Sigma-Aldrich (St. Louis, MO) and Life Technologies.

2.2. Confocal Imaging of A549 cells using LAURDAN

A549 (ATCC, CCL185™) cells were seeded in 35mm glass bottom dishes (7.5×10^5 cells/dish) and cultured in 2 mL DMEM-F12 (Sigma), 10% fetal bovine serum, at 37°C for 1, 4, 7, 10 and 14 days after confluence and without medium exchange for this time. Cells were incubated with LAURDAN using a stock solution of the probe in DMSO 4.4 mM and with a final concentration in the culture medium between 1.8 – 3.6 μM (final volume of DMSO at the culture medium was always below 0.5%). After addition of the probe, the cells were

incubated at 37°C for at least 2 hours. Prior to imaging, the culture medium was replaced by DMEM-F12 with 10% fetal bovine serum, HEPES 20 mM and without phenol red. To induce secretion of LB-like structures, LAURDAN labeled cells were incubated for 1 hour with 100 μM of ATP and isoproterenol. After this last step the supernatant was centrifuged for 10 minutes at 1000 ×g and 4°C to remove debris, followed by a final ultracentrifugation at 200000 ×g and 4°C for 15 min to pellet these organelles. The pellet was resuspended in buffer Tris 10 mM, 150 mM NaCl, pH 7.0 and then deposited in a microscope slide for observation.

A Leica TCS SP5 Laser confocal microscope, equipped with temperature and CO_2 control and spectral imaging capabilities was used to carry out the experiments. LAURDAN excitation was performed using a 405 nm laser source. LAURDAN fluorescent images were obtained using a 63× oil objective with 1.4 NA, with an image resolution of 512×512 pixel, and a pixel size in x and y of 0.0686μm, and z resolution of 1 μm. For the spectral phasor analysis the spectrum was recorded using 32 channels in a wavelength range from 416 to 728 nm (bandwidth was 9.78 nm). Raman contribution in our microscopy images is negligible compared with the fluorescence signal measured in our experiments. LAURDAN is an amphiphilic fluorescence probe whose fluorescence emission is sensitive to the dynamics of water molecules in the vicinity of its fluorescence moiety located at the lipid bilayer interface. If the extent of water relaxation around the probe increases (e.g., as in a gel-to-fluid phase transition), its fluorescence emission maximum shifts from 440 nm to 490 nm. A quantitative way to measure the extent of water dipolar relaxation (which in turn is related to the extent of hydration) at the membrane interface is using the Generalized Polarization function [28,39]. The LAURDAN Generalized Polarization function (GP) was obtained from the spectral images, using the classical GP function ($GP = (I_{440}-I_{490})/(I_{440}+I_{490})$). Spectral phasor and GP imaging processing were done using the SimFCS software (Laboratory for Fluorescence Dynamics, www.lfd.uci.edu/globals).

2.3. Multilamellar vesicle preparation (MLVs)

Proper aliquots of lipids dissolved in organic solvent ($CHCl_3$) were deposited in glass test tubes and dried using a vacuum oven. Dried lipids were hydrated with a buffer solution (10 mM HEPES, pH 7.0) at temperature above the lipid melting transition of lipids (or those of their mixtures). The total concentration of lipids in MLVs suspension was 1 mM. The lipid composition in the MLVs suspensions were: dipalmitoylphosphatidylcholine (DPPC), dioleoylphosphatidilcholine (DOPC), or DPPC/cholesterol (Chol) 30% mol. The samples were labeled with LAURDAN (0.5% mol with respect to the total phospholipid concentration) by premixing the probe with the lipids in organic solutions. Fresh batches of MLVs were prepared before each measurement.

2.4. Spectral phasor plot analysis

The fluorescence spectra at each pixel from the LAURDAN fluorescence spectral images were Fourier transformed, as previously described [1,2]. Briefly, the LAURDAN spectrum obtained for each pixel is transformed using the following mathematical expressions:

$$\text{x coordinate} = G = \frac{\Sigma_\lambda I(\lambda).\cos(2\pi n(\lambda - \lambda i)/L)}{\Sigma_\lambda I(\lambda)} \qquad (1)$$

$$\text{y coordinate} = S = \frac{\Sigma_\lambda I(\lambda).\sin(2\pi n(\lambda - \lambda i)/L)}{\Sigma_\lambda I(\lambda)} \qquad (2)$$

where $I(\lambda)$ is the intensity at each channel step of the spectrum (32 steps), n is the number of the harmonic and L the length of the spectrum taken (728–416 = 312 nm for our experiments). The x and y coordinates (G and S, see equation 1 and 2) obtained are plotted in a scatter plot called the Fourier space. G and S take values between 1 to −1 and their position on the spectral phasor plot is simultaneously related to the center of mass and the full width of the half maximum (FWHM) of the spectrum.

From the data analysis it is possible to identify that the position of the phasor is defined by the phase angle and the modulus of the data. The final position of the spectrum at each pixel occupies a place in the plot related to the radial position and the angle from the phasor plot origin (1,0). The angular position in the phasor plot is related to the center of mass of the emission spectrum. For example, considering two spectra A and B with the same FWHM but different center of mass, i.e. B is red shifted respect to A. If the point representing the spectrum A is located at (S, G) equal to (0,0.9), the point representing the spectrum B will be counter clockwise rotated towards the coordinate (−1, 0) in the same circle of the phasor plot where the spectrum A is located (Figure S1). The radial position in the phasor plot on the other hand depends on the spectrum's FWHM. If we now consider a third spectrum C having the same center of mass as that of A but a broader width, the point representing spectrum C will move toward the center of the plot along the radius of the circumference (Figure S1).

To identify the pixels of interests in the images we used a cursor diagram which allows us to select the pixels coming from the LB-like structures (see for example Figure 2 in the results section).

2.4.1 Correlation experiments between LAURDAN and ABCA3-GFP—

LAURDAN fluorescence information from LB-like structures was also correlated through the spectral phasor approach with a specific molecular indicator for LB (ABCA3-GFP [38], plasmid generously provide by Prof. Inagaki, University of Tokyo)(see Figures S2). Additional information concerning the methods used to perform these experiments is described in the supplementary material section.

2.5. Data reproducibility and statistics

The experiments were performed by three independent biological replicates, and for each replicate 10 images were acquired in order to perform the statistical analysis. Data are shown as means ± standard deviation (SD) and were analyzed using the ANOVA and Tukey

post-test. All the samples showed normal distributions as judged by the Kolmogorov-Smirnov test. A p<0.05 was considered statistically significant. Statistical analysis was realized using GraphPad Software, Inc.

3. Results

3.1. Time dependent size changes of lamellar body-like structures in A549 cells

Figure 1A shows representative brightfield and fluorescent confocal images of LAURDAN labeled LB-like structures at 1, 7 and 14 days in culture post-confluence. The fluorescence images from this figure were used to determine the size (as diameter) of LB-like structures. In Figure 1B, the measured sizes are plotted as a function of post-confluence days. Figure 1B shows that LB-like structures increase their size, with significant differences between the first and subsequent days of culture. In order to gain a detailed understanding of this process, histograms showing the size distribution for days 1, 7 and 14 are presented in Figure 1C. Interestingly, the histogram's size distribution becomes broader from day 1 to 7, but narrows again at day 14 (see Table S1).

To link the nature of the subcellular structures shown in Figure 1 with LBs we performed a set of control experiments with a specific LB molecular marker, the ABCA3 transporter tagged with GFP (ABCA3-GFP) (see Figure S2). Specifically, regular co-localization and SP analyses were performed between LAURDAN and ABCA3-GFP using fluorescence and brightfiled microscopy (Figure S2). All these results support the LB-like nature of the structures presented in Figure 1 (see discussion in supplementary material).

In addition, others control studies were performed concerning cell integrity/viability, as well as an evaluation of the glucose/lactate content in the culture medium over time. These last results indicate that there are not significant differences in the viability of the cells between days 1 to 14, showing also that membrane integrity is preserved (Figure S3 and Table S3). Additionally, the concentration of glucose and lactate measured in the medium at 7 and 14 days post-confluence discard any possibility of cell starvation during the time of our experiments (see Figure S4).

3.2. Size of lamellar body-like structures and membrane hydration

LAURDAN spectral phasor analyses of LB-like structures were performed in cell cultures with the aim to link size changes with changes in their overall (membrane) hydration. Figure 2A shows the spectral phasor's first harmonic for LB-like structures in a set of images at different post-confluence days at 37°C. From the data obtained, it is possible to correlate the position of the pixels-which fall in a linear trajectory as the post-confluence days augment-with the extent of water relaxation experienced by the probe inserted in these organelles. Figure 2B shows representative fluorescence intensity (first row, from left to right) and the corresponding Fourier transformed images using the pixels selected in the spectral phasor plot (second row, see Methods and Table S2 for details). The third column of Figure 2B shows a zoom of the Fourier transformed images showing mainly intracellular LB-like structures. Inspection of the Fourier transformed images shows that the increase in the number and size of these organelles correlates with increased levels of blue pixels as the

days of post-confluence progress. Altogether the information from Figure 2A and B clearly indicates a decrease in the hydration state of LB-like structures at longer post-confluence days. Figure 2C shows a blue shift in the average normalized LAURDAN spectra obtained from full images (LB-like structures plus other membranous structures in the cell) at different days of post-confluence.

A plot of the ratio between the pixel fractional intensities (FI) obtained for LB-like structures (mainly represented by the blue and green cursors in Figure 2A; see Figure S5) and the size of LBs versus days of post-confluence is shown in Figure 3A. The FI/size ratio is a parameter that normalizes the pixel fractional intensities by the size of these organelles. Accordingly, the data corroborates that time is indeed an important parameter influencing the overall probe response, which differentially responds to the state of hydration of these intracellular membranous structures at different post confluence days.

Correlation plots between the pixel fractional intensity (FI) obtained from LB-like structures (blue and green cursors respectively, from Figure 2A) and their size (data in Figure 1B) at different post-confluence days are presented in Figure 3B and C. These plots indicate a two-step process. As shown in Figure 3B, from days 1 to 7 these organelles augment their size without a significant change in the LAURDAN spectral parameters. However, after day 7, intracellular LB-like structures show a significant variation in the spectral characteristics of the probe with their size. In other words, first these intracellular membranous structures increase their size without significant changes in their global hydration, but after 7 days they become dehydrated (Figure 3B). It is important to notice that the plot obtained from the green cursor shows almost the same trend with slight differences in the time where dehydration occurs (Figure 3C).

Finally, we sought to compare the spectral phasor results with the classical LAURDAN Generalized Polarization (GP) function [28,39]. LAURDAN GP values were calculated at each pixel using the spectral images at different post-confluence days. Figure 4 shows a representative GP image and histograms obtained at 14 days post-confluence. Notice that two Gaussian distributions were able to fit the histograms, corresponding to intracellular LBs (GP_2) and other membranous structures (GP_1), see Table 1. Interestingly the GP_2 values increase with the time of post-confluence, indicating a reduction in the extent of water relaxation at longer post confluence days. This result agrees with the data interpretation from Figures 2A and B.

3.3. Comparative analysis between LB-like structures and lamellar model membranes

In order to further explore the membrane organization of intracellular LB-like structures *in cellulo,* comparative experiments were performed using different well-characterized lamellar membrane model systems relevant to LB-like structures composition. Figures 5A and B show the spectral phasor analysis for different lamellar models displaying solid ordered (s_o, DPPC at 37°C), liquid disordered (l_d, DOPC at 37°C), liquid ordered (l_o; DPPC+30% cholesterol, at 37°C) phases and intracellular LB-like structures plus other cell membranes from A549 cells at 14 days post confluence. Figure 5A and B show that the pixels coming exclusively from A549 membranes, other than LB-like structures, fall in the middle of the trajectory of the line obtained as a linear combination of l_d and l_o phases. For intracellular

LB-like structures, however, the associated pixels fall over this trajectory but outside the limit imposed by our I_o phase reference (i.e. DPPC+ 30% cholesterol; light blue circle in Figure 5A and B). Additionally as indicated in Figure 5C intracellular LB-like structures show a relatively bluer spectrum compared with the rest of the samples. Another important observation from these experiments is the fact that the $I_d - s_o$ trajectory shows a different slope with respect to that for $I_d - I_o$, showing the sensitivity of the method to the presence of cholesterol in the membranes [40].

Finally, Figure 5D shows the spectral phasor analysis for *secreted* LB-like structures from A549 cells, including the trajectories previously identified in Figure 5A and B. Notice that these secreted organelles were labeled with LAURDAN prior secretion (see material and methods). The data shows that the LAURDAN fluorescence emission from secreted LB-like structures also falls in the $I_d - I_o$ trajectory but in a different position, much closer to the I_o reference. In other words, the fluorescence observed in pixels from secreted organelles are red-shifted with respect to that observed in the intracellular environment, indicating an increase in the extent of hydration of these membranous structures during the secretion process.

4. Discussion

By using state-of-the-art fluorescence microscopy experiments/analyses we were able to characterize unexplored features regarding the time evolution of intracellular LB-like structures in live A549 cells. Our first result shows that there is a time-dependent increase in the size of intracellular LB-like structures (Figure 1). This process is not discrete as indicated by the histograms shown in Figure 1C, suggesting a heterogeneous growth of these intracellular organelles vs. time. To the best of our knowledge this is the first time that this phenomenon has been quantitatively characterized at *in cellulo* conditions. Shapiro et al. previously showed that A549 cells changes the number and composition of the lamellar body-like structures with the degree of confluence [31]. We considered this observation and we kept the cells for 14 days post-confluence without medium exchange, since epithelial cells need some basal level of paracrine signaling to organize their functions [41]. In Caco-2 cell line for example, it was demonstrated that the subsequent days after seeding are relevant to reach the level needed of paracrine signaling to allow the maximum activity for some proteins in the ABC transporter family [42].

4.1. Time evolution of intracellular LB-like structures: size and hydration

Several models have been postulated proposing the control of the organelle size as an important parameter for secretion such as i) a precursor limit model (i.e. cell size), ii) a constant growth model (i.e. a relationship between the growth of the cell and its organelles over time) or iii) a feedback model based on size measurements (which in principle involves a "molecular sensor") [43]. The last model specifically posits that in membrane-bound organelles pumps and channels are linked to ion fluxes, which depend on the surface area and shape of the organelle, serving as size indicators. On the other hand, Perez-Gil [9], previously proposed a model for intracellular LB maturation uniquely based on the ultrastructure of LBs obtained from TEM results and biochemical information about the

requirement of some important proteins for the process like ABCA3 and SP-B. Specifically, the author suggested that the accumulation of lipids in LBs, i.e. throughout the ATP consuming process by ABCA3 in combination with SP-B, causes different membrane lamellar organizations (concentric or parallel), which in turn is related to their maturation state. However, none of the intracellular maturation models enumerated above can provide an account for the differential changes of hydration as observed in our studies for LB-like structures at *in cellulo* conditions. The experiments presented in Figure 2 (and Table 1) show an effective decrease in global hydration [30] of intracellular LB membranes, particularly noticeable at longer post-confluence days. This decrease is reflected by the linear trajectory in the phasor plot (Figure 2A).

Interestingly, the two-step process shown in Figure 3 (B and C) indicates that these organelles first develop in size without significant changes in hydration, but that after reaching a certain dimension the hydration state of intracellular LB-like structures plummets with organelle size. From this result it is possible to argue that intracellular LBs are developing differentially, and that when a given lipid/protein/water ratio is reached the organelles can be secreted. Although speculative at this stage, the hydration state of intracellular LBs could be an important parameter to explain unresponsive populations of intracellular LBs to Ca^{2+} signaling [20], i.e. a mechanism to identify and select a particular population of intracellular LBs for release and hold others in the cytosol while they acquire the physical properties that allow secretion to the extracellular space. The relatively higher hydration state measured for secreted LB-like organelles respect to intracellular population could be important to explain this phenomenon (see discussion below). On the other hand, it interesting to highlight the straightforward correlation between the significant dehydration into LB-like structures after 7 days of post.-confluence with the activity peak reported for some ABC transporter members in other epithelial cells [41]. The Caco-2 cells somehow need some kind of extracellular signaling to perform their "regular physiological" function.

4.2. Implications of LB-like structures hydration before and after secretion

The change in the hydration state observed in LB-like structures before and after secretion (Figure 5D) may offer relevant clues about the role of intracellular water during this process. For instance, the ejection of intracellular LBs (which are dehydrated with respect to secreted LBs) into a relative diluted medium (like the epithelial lining fluid) could be favored by entropic changes caused by hydration. This hydration process could also play a role during the transformation of LBs after secretion into tubular myelin [20] or the spreading of these organelles at the alveolar interface [24]. Another biological example showing a similar entropy-driven process is the super-contraction of spider silk [44]. The recoil of specific silk proteins originated by their molecular reorganization controls this process, which largely depends on the level of water in the system.

A recent publication Cerrada *et al.* [25] reported, based on LAURDAN GP measurements, that at physiological temperatures the relaxation experienced by the probe in intracellular LBs, from rat ATII cells, is similar to that observed for secreted LBs. This result is different from the ones we report using A549 cells. In our experiments we observed that secreted LB-like structures show a more relaxed LAURDAN fluorescence emission (i.e. higher

hydration) with respect to the intracellular population. Although this difference can be trivially attributed to the different nature of the cellular lines utilized in both studies [31,32], we have a few concerns about the GP data presented by the authors on secreted LBs (Figure 3B in reference [25]). Specifically, these authors used very low concentrations of secreted LBs in their fluorescence measurements and performed a subtraction of the Raman peak (which in a regular fluorimeter represents approximately twice the noise of the equipment). Under these very low signal (and noisy) conditions a remaining contribution of Raman (which is blue shifted respect to LAURDAN emission) can increase the measured GP values. This observation may offer a plausible explanation about the observed differences.

Cerrada *et al.* [25] also discussed a potential mechanism on LBs spreading after secretion. These authors postulate that the energy accumulated during intracellular LB biogenesis (ATP consumption catalyzed by ABCA3 transporters) can be somehow utilized by LBs adopting a high energy –dehydrated- structures for a subsequent spreading at the alveolar interface. Specifically, they suggested that this energized state existing in LBs, which remains unaltered during secretion, could be released by a disruption of LBs outer membrane driving their subsequent spreading into the alveolar interface. Without invoking additional steps (which remain to be proven) we suggest a simpler view based on a simple entropy-driven thermodynamic mechanism. Specifically we hypothesize that the low entropy state gained by the system during biogenesis is already exploited during secretion. This hypothesis is based on two important observations: i) the progressive dehydration of intracellular LB-like structures observed at long post-confluence days, and ii) the increased hydration state displayed by these organelles upon secretion. In other words, the entropy of the system may increase during LB secretion to the alveolar lining fluid assisting subsequent transformations of the material (either its transformation to tubular myelin or its spreading to the alveolar interface).

4.3. Comparison between LB-like structures and artificial lamellar membrane models

Comparisons of the emission spectral features of well-defined lamellar membrane phases in the spectral phasor plot show that intracellular LB-like structures differ from the selected lamellar membrane models used in our experiments (Figure 5). The two trajectories defined by the dashed lines in the spectral phasor plot (Figure 5A and B) define the limits and the position where a discrete emission of LAURDAN should fall assuming a linear combination of l_d–s_o or l_d–l_o phases. The possibility to define these trajectories is a powerful feature of the phasor plot method, absent in the GP function analysis, which requires a predefined model to fit the data [28]. For example, it is difficult to unambiguously interpret the physical features of our compositionally complex LB-like structures membranes solely based on GP values obtained in model membranes displaying s_o (gel) or l_o phase states. As previously reported, the GP values obtained in these model systems are very close, indicating a very low extent of solvent relaxation in both cases [39,45,46]. This problem is circumvented by the spectral phasor plot analysis (Figure 5, which simultaneously consider the spectra center of mass and width), defining characteristic trajectories that depend on specific phase transformation of the system.

Since LBs, as well as other cellular membranes, contain different cholesterol levels, the l_d–l_o trajectory emerges as a relevant case to analyze. After the analysis we found two interesting features. First, in agreement with previous observations [2,40], cell membranes other than LB-like structures (green cursor, Figure 5A and B) fall between the limits of the l_d–l_o trajectory defined by the lamellar model membranes used as references (red and purple cursors respectively, Figure 5A and B). This observation indicates that the physical features of these membranes can be described as a linear combination of the l_d and l_o phases as observed in our reference membrane models. Second, although intracellular LB-like structures (light blue cursor, Figures 5 and B) fall in the l_d–l_o trajectory, the values observed are outside its limits. Thus, the spectral phasor results support the existence of an unusual dehydrated state for intracellular LB-like membranous structures compared with relevant lamellar model membranes. We put forward two hypotheses to interpret this observation: i) a lamellar configuration exists in intracellular LB-like structures, but contains much higher amounts of cholesterol than our l_o phase reference model membrane, or ii) intracellular LB-like structures may display a more complex membrane organization, induced for example by the presence of relevant lipids and proteins in a very dehydrated/crowded environment. The fact that the amount of cholesterol in LBs [47] is much lower than that for DPPC +cholesterol 30% mol supports this hypothesis (ii).

It is well known from previous reports that these specialized organelles contain a very low water/mass molar ratio [47], which is in line with the dehydrated state obtained in our experimental results. Theoretical calculations considering the spatial dimensions of a phospholipid and water molecules indicate that inside secreted LBs there are only 6–7 water molecules per phospholipid, which is in agreement with reported experiments [47]. However, this calculation does not take into account the water involved in the hydration shell of proteins, ions and small solutes. Based on the data reported by Grathwohl and collaborators [47], a LB contains approximately 2.6×10^5 protein molecules, which means that around 7.3×10^8 additional water molecules are taken from free water (i.e. involved in the hydration shell of the proteins). All these numbers support the existence of a very crowded environment in the intracellular LBs with an extremely low hydration state as also suggested by the results of Cerrada *et al.* [25].

Molecular crowding is a relevant concept addressing potential limitations of the classical van´t Hoff solution theory, which is mostly applicable to dilute solutions [48]. In systems displaying molecular crowding, the amount of free (liquid) water is low. Under these conditions lipid membranes may display changes in their supramolecular organization, e.g. transitions from lamellar to non-lamellar structures (a phenomenon called lyotropic mesomorphism) [49,50]. The number of water molecules per phospholipid required to stabilize a lamellar lipid structure is approximately 20, of which around 6–7 water molecules are highly coordinated with the lipids (i.e. cannot be crystalized above −100°C) [51]. Considering the low hydration state of intracellular LB-like structures *in cellulo* compared with the secreted ones and the differences observed with a lamellar model system (Figure 5) we hypothesize the existence of membranous structures other than purely lamellar existing in intracellular these organelles under these conditions. Some compositional facts support this possibility: phospholipids such as phosphatidylethanolamine (PE), phosphatidylserine (PS) and phosphatidylinositol (PI), (i.e. 7% PS+PI are reported in LBs [47]) can promote

non-lamellar phases in conditions characterized by very low water content, low pH and high Ca^{2+} concentrations [52]. Additionally, non-lamellar structures can be stabilized by the presence of SP-B and SP-C, as reported in a model system composed of DOPC:DOPE [53]. Indeed *in vitro* experiments using extract of broncho-alveolar lavages from sheep lungs reported by Teubner *et al.* demonstrated lyotropicmesomorphism induced by the percentage of water in the system [54]. Although appealing, it is important to emphasize that this is an *ad hoc* hypothesis that requires additional experimental data, beyond the scope of this manuscript, to be conclusive. Interestingly, however, Cerrada *et al.* recently suggested the presence of non-lamellar phases in secreted LBs [25] based in ATR-FTIR experiments. This information supports our *ad hoc* hypothesis and complements our observations. For instance, the different position observed in the phasor plot for secreted LB-like structures respect to intracellular LB-like structures outside the I_d–I_o trajectory defined by our membrane model may be interpreted as a linear combination between contributions from lamellar and non-lamellar structures in LBs before and after secretion.

Finally, the GP values we measured in intracellular LB-like structures (Figure 4, Table 1) are significantly higher than those for I_o-like phases reported from giant vesicles composed of pulmonary surfactant (the very final material after LB secretion) obtained from murine lung lavages [55], suggesting important differences with this material. These last results are in agreement with recent observations from Cerrada *et al.*, where they perform a comparative study using different experimental approaches between secreted LBs and pulmonary surfactant obtained from broncho-alveolar lavages [25].

4.4. A model to interpret the spectral phasor plot for LB-like structures

The membrane cavities model introduced by Parasassi and coworkers [29] postulates that LAURDAN can sense a few molecules of water (i.e. 0 to 5, however the significant statistic is between 0–3) in their vicinity with a particular relaxation time (which is in the order of nanoseconds). Here we discuss how this model could be applied to the data obtained for LB-like structures using a continuum cursor diagram scheme. Our aim is to quantitatively explain changes in hydration over time for LB-like structures at *in cellulo* conditions. Considering the properties of the spectral phasor and the Parasassi model addressed above, we may reasonably postulate that the LAURDAN emission observed in LB-like structures is explained by a linear combination of discrete states reflecting the presence of 0, 1, 2 or 3 water molecules. These states should fall in the line joining the limits, i.e. 0 (completely mature and dehydrated LBs) and 3 (partially hydrated and immature LBs) water molecules. Notice that a new cursor scheme is created to analyze the data presented in Figure 2A (shown as Figure 6A). As LBs start to increase their size, LBs membrane shows pixels with different linear combination of red and purple cursors (represented by green, light blue and blue colors in Figure 6A). At post-confluence day 14 the interior is completely purple, indicating that LB-like structures membrane evolved by dehydrating their structure (Figure 6B).

5. Conclusions

The results and conclusions in this study tackle an important aspect for biological systems: the impact of the heterogeneous state of hydration, existing in organelles in particular and the cell interior in general [56], on structural and dynamical aspects of cells. Although recognized by several researchers, the phenomenon of molecular crowding and its effects on the physicochemical properties of the intracellular environment is still not fully incorporated in the canonical models that describe the cell [57]. We found strong evidence that LB-like structures in A549, which are particularly crowded lipid-rich organelles, noticeably show a time dependent dehydration at *in cellulo* conditions. Upon secretion, this situation is partially reverted. These observations support the contention that cell processes depend on the maintenance of a low entropy state [58,59]. Finally, the extreme sensitivity of LAURDAN spectral imaging and the spectral phasor analysis opens the possibility of effectively comparing *in cellulo* LB structure with canonical lamellar model membrane systems. The observations obtained in this part of the study challenge the current view of purely lamellar structures existing in intracellular LB-like membranes. In general terms this result raises an important question related to the role of membrane lyotropic mesomorphism in the highly crowded intracellular environment.

Supplementary Material

Refer to Web version on PubMed Central for supplementary material.

Acknowledgments

Abbreviations

LAURDAN	6-dodecanoyl-2-dimethylaminonaphthalene
LBs	lamellar bodies
GP	Generalized Polarization function
FWHM	full width of the half maximum
MVB	multivesicular bodies
PS	pulmonary surfactant
ABCA3	ATP-binding cassette transporter A3

References

1. Fereidouni F, Bader AN, Gerritsen HC. Spectral phasor analysis allows rapid and reliable unmixing of fluorescence microscopy spectral images. Opt. Express. 2012; 20:12729. [PubMed: 22714302]

2. Golfetto, O.; Hinde, E.; Gratton, E. The Laurdan Spectral Phasor Method to Explore Membrane Micro-heterogeneity and Lipid Domains in Live Cells. In: Owen, DM., editor. Methods Membr. Lipids SE - 19. New York: Springer; 2015. p. 273-290.

3. Bagatolli LA, Ipsen JH, Simonsen AC, Mouritsen OG. An outlook on organization of lipids in membranes: searching for a realistic connection with the organization of biological membranes. Prog. Lipid Res. 2010; 49:378–389. [PubMed: 20478336]

4. Bagatolli LA, Mouritsen OG. Is the fluid mosaic (and the accompanying raft hypothesis) a suitable model to describe fundamental features of biological membranes? What may be missing? Front. Plant Sci. 2013; 4:457. [PubMed: 24312108]

5. Matsumura Y, Sakai H, Sasaki M, Ban N, Inagaki N. ABCA3-mediated cholinephospholipids uptake into intracellular vesicles in A549 cells. FEBS Lett. 2007; 581:3139–3144. [PubMed: 17574245]

6. Shpilka T, Elazar Z. Lipid droplets regulate autophagosome biogenesis. Autophagy. 2015; 11:2130–2131. [PubMed: 26513372]

7. Henne WM. Organelle remodeling at membrane contact sites. J. Struct. Biol. 2016:1–5. In press.

8. Hatasa K, Nakamura T. Electron microscopic observations of lung alveolar epithelial cells of normal young mice, with special reference to formation and secretion of osmiophilic lamellar bodies. Zeitschrift Für Zellforsch. Und Mikroskopische Anat. 1965; 68:266–277.

9. Pérez-Gil J. Structure of pulmonary surfactant membranes and films: the role of proteins and lipid-protein interactions. Biochim. Biophys. Acta. 2008; 1778:1676–1695. [PubMed: 18515069]

10. Beers MF, Mulugeta S. Surfactant protein C biosynthesis and its emerging role in conformational lung disease. Annu. Rev. Physiol. 2005; 67:663–696. [PubMed: 15709974]

11. Dietl P, Liss B, Felder E, Miklavc P, Wirtz H. Lamellar Body Exocytosis by Cell Stretch or Purinergic Stimulation: Possible Physiological Roles, Messengers and Mechanisms. Cell. Physiol. Biochem. 2010; 25:1–12. [PubMed: 20054140]

12. Islam MN, Gusarova GA, Monma E, Das SR, Bhattacharya J. F-actin scaffold stabilizes lamellar bodies during surfactant secretion. Am. J. Physiol. - Lung Cell. Mol. Physiol. 2014; 306:L50–L57. [PubMed: 24213916]

13. Singh TK, Abonyo B, Narasaraju TA, Liu L. Reorganization of cytoskeleton during surfactant secretion in lung type II cells: a role of annexin II. Cell. Signal. 2004; 16:63–70. [PubMed: 14607276]

14. Chander A, Gerelsaikhan T, Vasa PK, Holbrook K. Annexin A7 trafficking to alveolar type II cell surface: Possible roles for protein insertion into membranes and lamellar body secretion. Biochim. Biophys. Acta - Mol. Cell Res. 2013; 1833:1244–1255.

15. Gerelsaikhan T, Vasa PK, Chander A. Annexin A7 and SNAP23 interactions in alveolar type II cells and in vitro: A role for Ca2+ and PKC. Biochim. Biophys. Acta - Mol. Cell Res. 2012; 1823:1796–1806.

16. Gerelsaikhan T, Chen X-L, Chander A. Secretagogues of lung surfactant increase annexin A7 localization with ABCA3 in alveolar type II cells. Biochim. Biophys. Acta - Mol. Cell Res. 2011; 1813:2017–2025.

17. Haller T, Ortmayr J, Friedrich F, Völkl H, Dietl P. Dynamics of surfactant release in alveolar type II cells. Proc. Natl. Acad. Sci. U. S. A. 1998; 95:1579–1584. [PubMed: 9465058]

18. Haller T, Auktor K, Frick M, Mair N, Dietl P. Threshold calcium levels for lamellar body exocytosis in type II pneumocytes. Am. J. Physiol. 1999; 277:L893–L900. [PubMed: 10564173]

19. Dietl P, Haller T, Mair N, Frick M. Mechanisms of surfactant exocytosis in alveolar type II cells in vitro and in vivo. News Physiol. Sci. 2001; 16:239–243. [PubMed: 11572929]

20. Dietl P, Haller T. Exocytosis of lung surfactant: from the secretory vesicle to the air-liquid interface. Annu. Rev. Physiol. 2005; 67:595–621. [PubMed: 15709972]

21. Nicholas TE, Power JH, Barr HA. Surfactant homeostasis in the rat lung during swimming exercise. J. Appl. Physiol. 1982; 53:1521–1528. [PubMed: 6897548]

22. Dietl P, Frick M, Mair N, Bertocchi C, Haller T. Pulmonary consequences of a deep breath revisited. Biol. Neonate. 2004; 85:299–304. [PubMed: 15218287]

23. Hobi N, Siber G, Bouzas V, Ravasio A, Pérez-Gil J, Haller T. Physiological variables affecting surface film formation by native lamellar body-like pulmonary surfactant particles. Biochim. Biophys. Acta - Biomembr. 2014; 1838:1842–1850.

24. Ravasio A, Olmeda B, Bertocchi C, Haller T, Pérez-Gil J. Lamellar bodies form solid three-dimensional films at the respiratory air-liquid interface. J. Biol. Chem. 2010; 285:28174–28182. [PubMed: 20558742]

25. Cerrada A, Haller T, Cruz A, Pérez-Gil J. Pneumocytes Assemble Lung Surfactant as Highly Packed/Dehydrated States with Optimal Surface Activity. Biophys. J. 2015; 109:2295–2306. [PubMed: 26636941]

26. Vanhecke D, Herrmann G, Graber W, Hillmann-Marti T, Mühlfeld C, Studer D, Ochs M. Lamellar body ultrastructure revisited: high-pressure freezing and cryo-electron microscopy of vitreous sections. Histochem. Cell Biol. 2010; 134:319–326. [PubMed: 20809233]

27. Sueyoshi R, Tada K, Goto M, Tamai N, Matsuki H, Kaneshina S. Barotropic phase transition between the lamellar liquid crystal phase and the inverted hexagonal phase of dioleoylphosphatidylethanolamine. Colloids Surf. B. Biointerfaces. 2006; 50:85–88. [PubMed: 16697154]

28. Malacrida L, Gratton E, Jameson DM. Model-free methods to study membrane environmental probes: A comparison of the spectral phasor and generalized polarization approaches. Methods Appl. Fluoresc. 2015 In Press.

29. Parasassi T, Gratton E, Yu WM, Wilson P, Levi M. Two-photon fluorescence microscopy of laurdan generalized polarization domains in model and natural membranes. Biophys. J. 1997; 72:2413–2429. [PubMed: 9168019]

30. Bagatolli, LA. LAURDAN Fluorescence Properties in Membranes: A Journey from the Fluorometer to the Microscope. In: Mely, G.; Yves; Duportail, editors. Fluoresc. Methods to Study Biol. Membr. Vol. 13. Heidelberg: Springer-Verlag; 2012 Spring. p. 3-36.

31. Shapiro DL, Nardone LL, Rooney SA, Motoyama EK, Munoz JL. Phospholipid biosynthesis and secretion by a cell line (A549) which resembles type II alveolar epithelial cells. Biochim. Biophys. Acta (BBA)/Lipids Lipid Metab. 1978; 530:197–207.

32. Mason RJ, Williams MC. Phospholipid composition and ultrastructure of A549 cells and other cultured pulmonary epithelial cells of presumed type II cell origin. Biochim. Biophys. Acta - Lipids Lipid Metab. 1980; 617:36–50.

33. Foster KA, Oster CG, Mayer MM, Avery ML, Audus KL. Characterization of the A549 cell line as a type II pulmonary epithelial cell model for drug metabolism. Exp. Cell Res. 1998; 243:359–366. [PubMed: 9743595]

34. De Jiang R, Shen H, Piao YJ. The morphometrical analysis on the ultrastructure of a549 cells. Rom. J. Morphol. Embryol. 2010; 51:663–667. [PubMed: 21103623]

35. Nalayanda DD, Puleo C, Fulton WB, Sharpe LM, Wang TH, Abdullah F. An open-access microfluidic model for lung-specific functional studies at an air-liquid interface. Biomed. Microdevices. 2009; 11:1081–1089. [PubMed: 19484389]

36. Tatur S, Groulx N, Orlov SN, Grygorczyk R. Ca 2 + -dependent ATP release from A549 cells involves synergistic autocrine stimulation by coreleased uridine nucleotides. 2007; 2:419–435.

37. Mahto SK, Tenenbaum-Katan J, Greenblum A, Rothen-Rutishauser B, Sznitman J. Microfluidic shear stress-regulated surfactant secretion in alveolar epithelial type II cells in vitro. Am. J. Physiol. Lung Cell. Mol. Physiol. 2014; 306:L672–L683. [PubMed: 24487389]

38. Matsumura Y, Ban N, Ueda K, Inagaki N. Characterization and classification of ATP-binding cassette transporter ABCA3 mutants in fatal surfactant deficiency. J. Biol. Chem. 2006; 281:34503–34514. [PubMed: 16959783]

39. Parasassi T, De Stasio G, d'Ubaldo A, Gratton E. Phase fluctuation in phospholipid membranes revealed by Laurdan fluorescence. Biophys. J. 1990; 57:1179–1186. [PubMed: 2393703]

40. Golfetto O, Hinde E, Gratton E. Laurdan fluorescence lifetime discriminates cholesterol content from changes in fluidity in living cell membranes. Biophys. J. 2013; 104:1238–1247. [PubMed: 23528083]

41. Sambuy Y, De Angelis I, Ranaldi G, Scarino ML, Stammati A, Zucco F. The Caco-2 cell line as a model of the intestinal barrier: Influence of cell and culture-related factors on Caco-2 cell functional characteristics. Cell Biol. Toxicol. 2005; 21:1–26. [PubMed: 15868485]

42. Mailleau C, Capeau J, Brahimi-Horn MC. Interrelationship between the Na+/glucose cotransporter and CFTR in Caco-2 cells: Relevance to cystic fibrosis. J. Cell. Physiol. 1998; 176:472–481. [PubMed: 9699500]

43. Marshall WF. Organelle size control systems: From cell geometry to organelle-directed medicine. BioEssays. 2012; 34:721–724. [PubMed: 22760545]

44. Liu Y, Shao Z, Vollrath F. Relationships between super contraction and mechanical properties of spider silk. Nat Mater. 2005; 4:901–905. [PubMed: 16299506]

45. Parasassi T, Di Stefano M, Loiero M, Ravagnan G, Gratton E. Influence of cholesterol on phospholipid bilayers phase domains as detected by Laurdan fluorescence. Biophys. J. 1994; 66:120–132. [PubMed: 8130331]

46. Bagatolli LA, Gratton E. Two-Photon Fluorescence Microscopy Observation of Shape Changes at the Phase Transition in Phospholipid Giant Unilamellar Vesicles. Biophys. J. 1999; 77:2090–2101. [PubMed: 10512829]

47. Grathwohl C, Newman GE, Phizackerley PJR, Town M-H. Structural studies on lamellated osmiophilic bodies isolated from pig lung 31P NMR results and water content. Biochim. Biophys. Acta - Biomembr. 1979; 552:509–518.

48. Disalvo EA, Lairion F, Martini F, Tymczyszyn E, Frías M, Almaleck H, Gordillo GJ. Structural and functional properties of hydration and confined water in membrane interfaces. Biochim. Biophys. Acta - Biomembr. 2008; 1778:2655–2670.

49. Milhaud J. New insights into water-phospholipid model membrane interactions. Biochim. Biophys. Acta. 2004; 1663:19–51. [PubMed: 15157606]

50. Cullis PR, Hope MJ, Tilcock CPS. Lipid polymorphism and the roles of lipids in membranes. Chem. Phys. Lipids. 1986; 40:127–144. [PubMed: 3742670]

51. Ueda I, Yoshida T. Hydration of lipid membranes and the action mechanisms of anesthetics and alcohols. Chem. Phys. Lipids. 1999; 101:65–79. [PubMed: 10810926]

52. Cullis PR, De Kruijff B. Lipid polymorphism and the functional roles of lipids in biological membranes. Biochim. Biophys. Acta - Rev. Biomembr. 1979; 559:399–420.

53. Chavarha M, Loney RW, Rananavare SB, Hall SB. Hydrophobic Surfactant Proteins Strongly Induce Negative Curvature. Biophys. J. 2015; 109:95–105. [PubMed: 26153706]

54. Teubner JK, Gibson RA, McMurchie EJ. THE INFLUENCE OF WATER ON THE PHASE TRANSITION OF SHEEP LUNG SURFACTANT A POSSIBLE MECHANISM FOR SURFACTANT PHASE TRANSITIONS IN VIVO. Biochim. Biophys. Acta. 1983; 750:521–525. [PubMed: 6687437]

55. Bernardino De La Serna J, Hansen S, Berzina Z, Simonsen AC, Hannibal-Bach HK, Knudsen J, Ejsing CS, Bagatolli LA. Compositional and structural characterization of monolayers and bilayers composed of native pulmonary surfactant from wild type mice. Biochim. Biophys. Acta - Biomembr. 2013; 1828:2450–2459.

56. Thoke HS, Tobiesen A, Brewer J, Hansen PL, Stock RP, Olsen LF, Bagatolli La. Tight Coupling of Metabolic Oscillations and Intracellular Water Dynamics in Saccharomyces cerevisiae. PLoS One. 2015; 10:e0117308. [PubMed: 25705902]

57. Minton AP. How can biochemical reactions within cells differ from those in test tubes? J. Cell Sci. 2006; 119:2863–2869. [PubMed: 16825427]

58. Ling, GN. A physical theory of the living state: the Association-induction hypothesis. New York: Blaisdell Publishing Co, New York; 1962.

59. Schrodinger, E. What is life? The physical aspect of the living cell. Cambridge: Cambridge University Press; 1944.

Highlights

- LAURDAN spectral phasor analysis is a relevant tool to study membranes.

- Intracellular LBs-like structures grow first in size, followed by sharp dehydration.

- Secreted LBs-like structures are more hydrated than the intracellular ones.

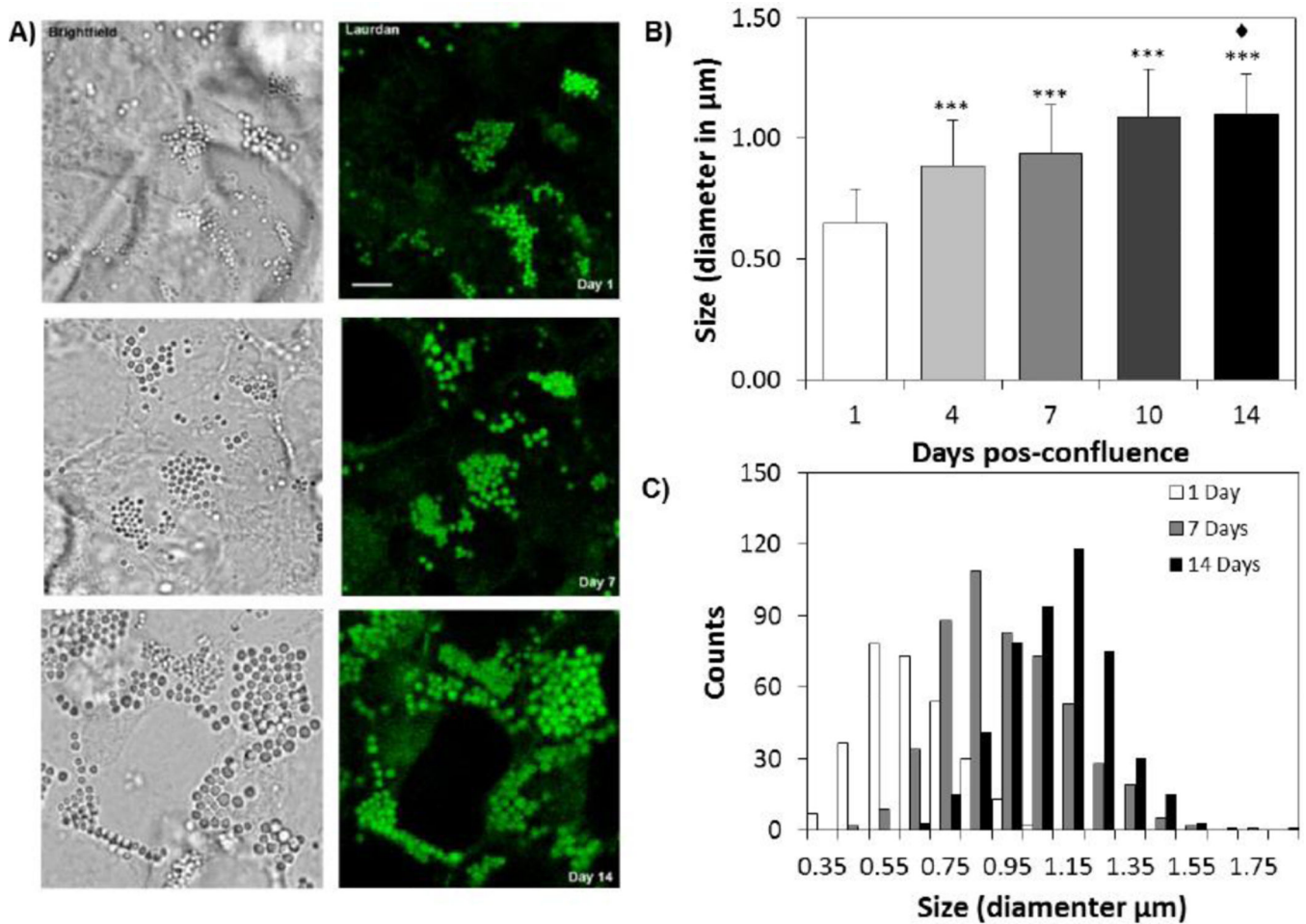- Non-lamellar phases can play a role in intracellular LB-like structures.

Figure 1. Size of Lamellar Body-like structures in A549 cells during post-confluence days
A) Representative bright-field and LAURDAN fluorescence images of LB–like structures in A549 cells at 1, 7 and 14 days post-confluence. B) Plot of the LB–like structures size (as diameter in μm) measured from the images presented in (A) at different stages of growth. C) Size distributions histogram of the LB–like structures at 1, 7 and 14 days of post-confluence. The values of the Gaussian fit are provided in Table S1. Values are represented as mean ± standard deviation. *** is statistical significant versus day 1 and ♦ is statistical significant versus day 7, with p<0.001. Bar scale represents 5μm.
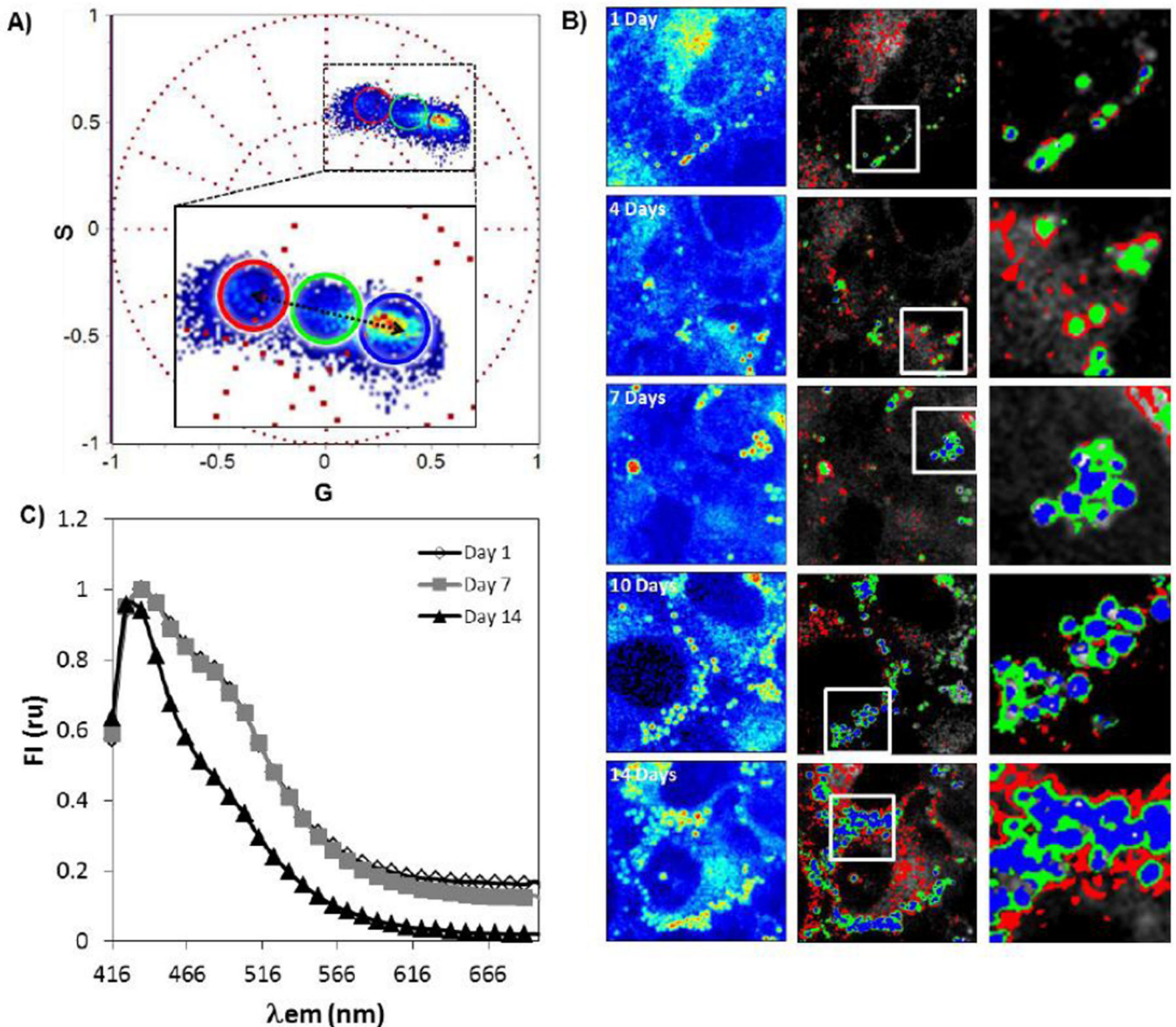
Figure 2. Spectral Phasor analysis of LAURDAN labeled intracellular LB–like structures from A549 cells

A) Plot of the first harmonic of the Fourier transformation of the LAURDAN spectrum in A549 cells, which includes the different days of post-confluence (1, 4, 7, 10 and 14). The diagram was generated selecting the adequate range in the image intensity histogram to exclusive select LB–like structures (see Figure S6). The center position and width values for each cursor are provided in Table S2. B) Representative confocal fluorescent images of A549 cells. The first column contains fluorescence intensity images of LAURDAN in a pseudo color scale (from blue to red). The second column shows pseudo colored images of LB–like structures containing A549 cells obtained by applying the cursor selection in the first harmonic plot shown in (A). The third column shows zooms of intracellular regions enriched in LB–like structures (obtained from the images in the center column). C)

LAURDAN spectra from the full images obtained at 1, 7 and 14 days of post-confluence. Bar scale represents 5μm.
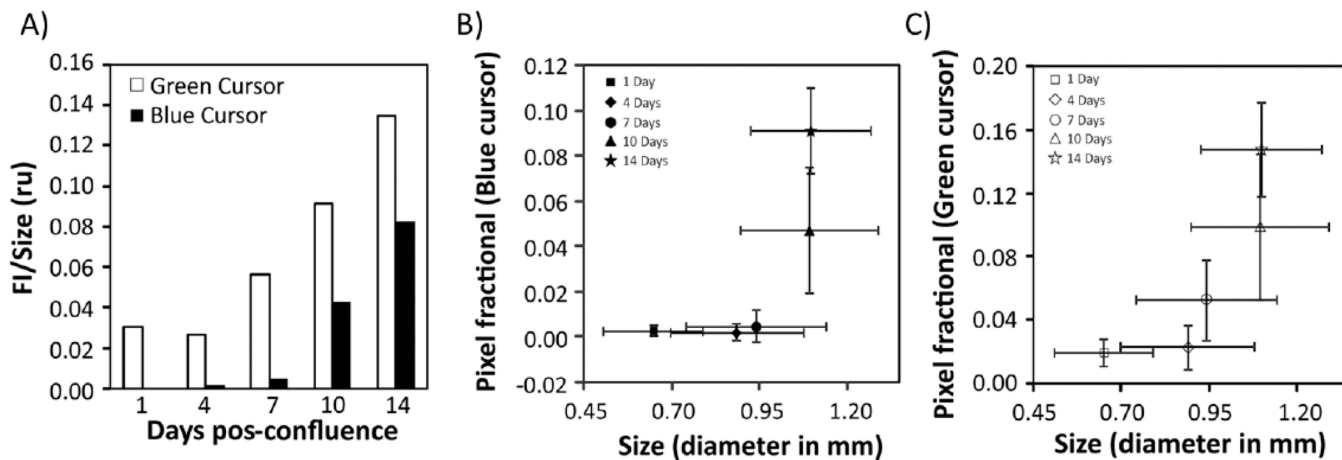
Figure 3. Correlation plots between LAURDAN fluorescence and size
A) LAURDAN fractional pixel intensity (green and blue cursors, obtained from Figure S5) normalized by LB–like structures size (FI/size) versus days of post-confluence. B and C) Plots of LAURDAN fractional pixels intensity (blue and green cursors, Figure S5) versus LB–like structures size. Values are represented as mean ± standard deviation.
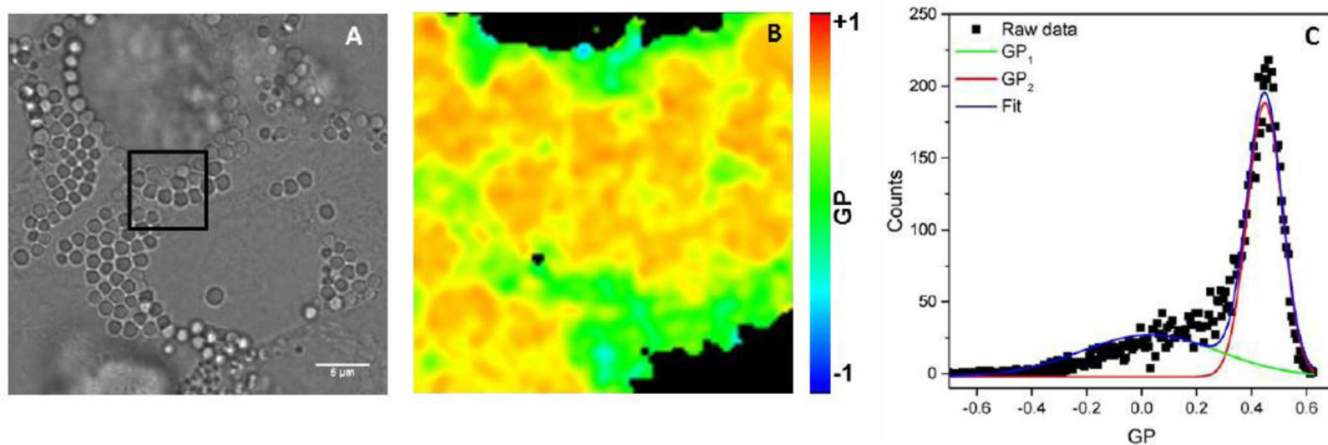
Figure 4. LAURDAN GP images of LBs in A549 cells at 14 days of post- confluence
A) Bright-field image where LB–like structures can be visualized. B) Generalized
Polarization (GP) image obtained from the ROI (black square) indicated in (A). The GP
image was calculated from the LAURDAN spectral images reported in Figure 2. C) GP
histogram at 14 days of post-confluence. The GP_1 and GP_2, and the full width at the half
maximum (FWHM) were determined by the fitting the GP histogram with two Gaussian
functions; see material and methods. The values of GP obtained at 1, 7 and 14 days are
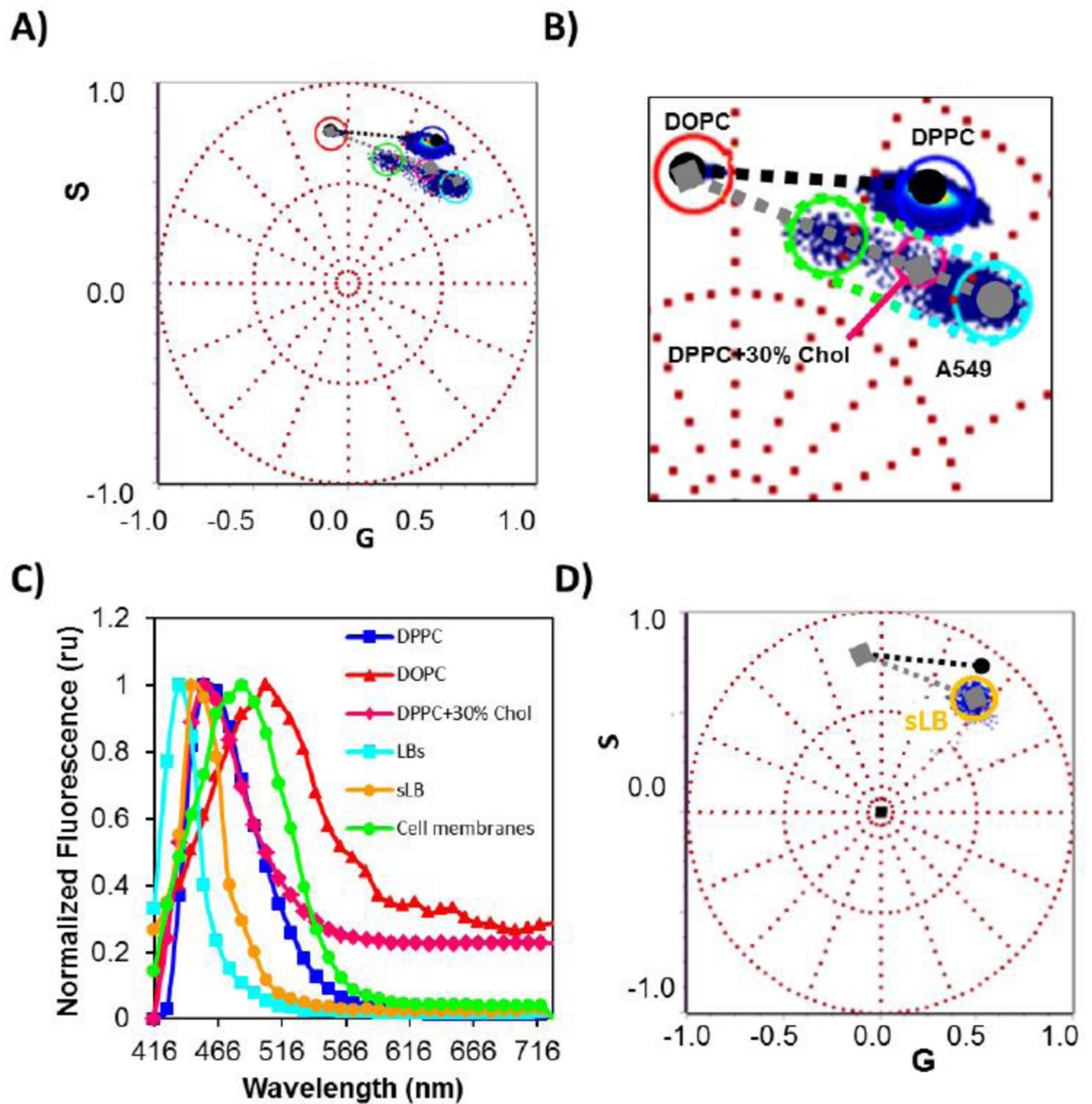provided in Table 1.

Figure 5. Comparative LAURDAN fluorescence spectral phasor analysis between LB–like structures and lamellar model membrane systems

A) Spectral phasor plot of LAURDAN in MLVs displaying different thermodynamic phases. Also the data for all labeled membranes of A549 cells (14 days of post-confluence are included). B) Zoom obtained from the Figure presented in A where the $l_o − l_d$ (grey dashed line) and $s_o − l_d$ (black dashed line) trajectories are shown. C) LAURDAN emission spectra obtained from intracellular (LB–like structures) and secreted LB–like structures (sLB) plus membranes for A549 cells at 14 days post-confluence and MLVs displaying l_o, s_o and l_d phases. D) Phasor plot analysis of LAURDAN labeled LB–like structures after secretion

(sLB, denoted with the orange cursor). The $s_o - l_d$ and $l_o - l_d$ trajectories shown in B are also included. Notice that the sLB distribution is located inside the trajectory defined by our l_d–l_o references, i.e. the emission spectrum of sLBis red shifted respect to the intracellular LB–like structures.
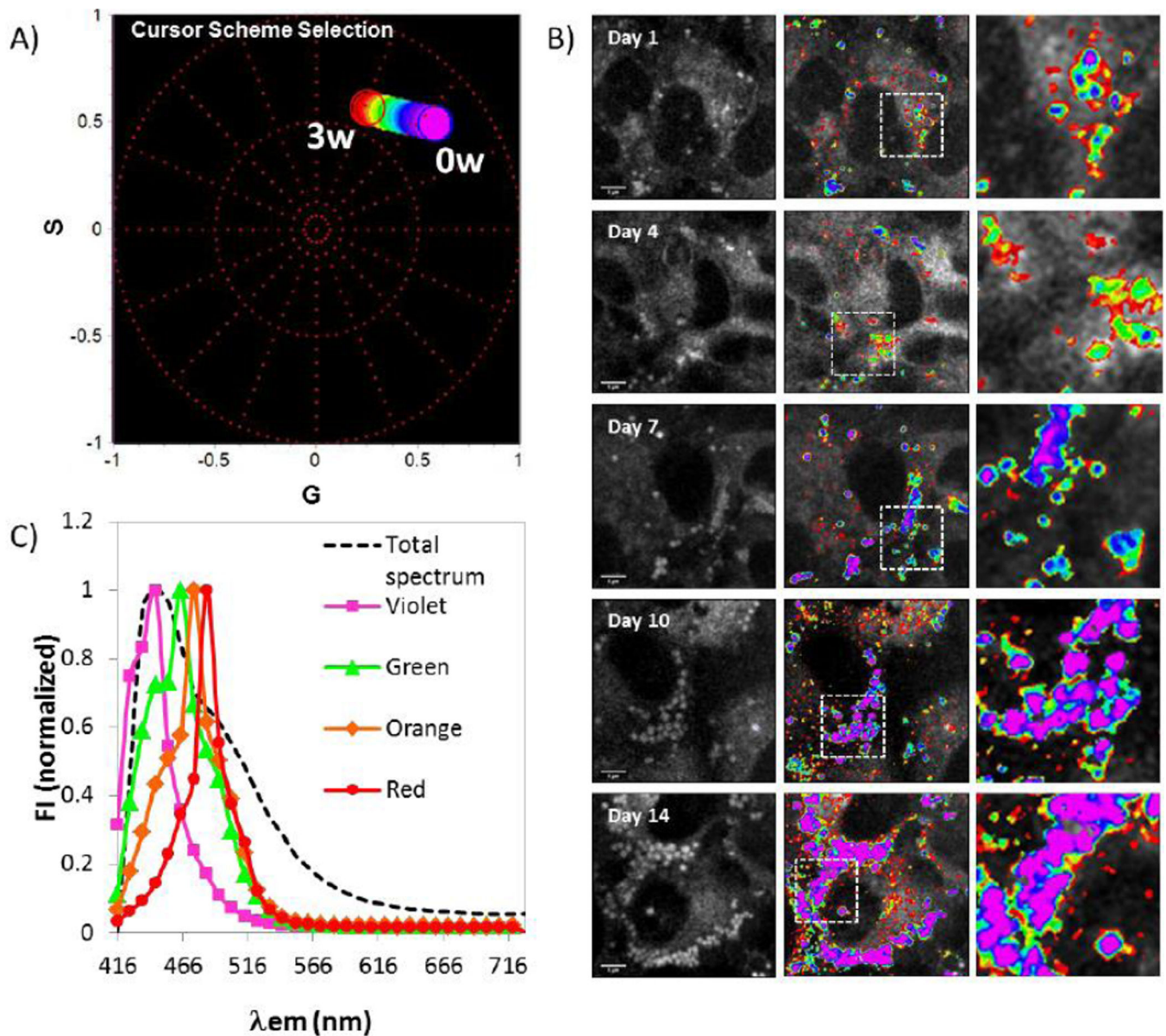
Figure 6. Spectral phasor analysis of LAURDAN emission from intracellular LB–like structures according to the "cavities" model (see text)
A) Cursor design of the pixels of LAURDAN in cell at different stages (3w and 0w, referring to the number of water molecules). B) Fluorescence intensity and pseudo color reconstruction images of LAURDAN emission in intracellular LB–like structures. The pseudo colored images were obtained by applying the cursor selection (violet, green, orange and red) in the first harmonic plot shown in (A). C) Emission spectra of LAURDAN at pixels selected with the different cursors (violet, green, orange and red). Bar scale represents 5μm.

Table 1

GP values obtained at different post-confluence days

Values of the GP were taken from the same spectral images of the spectral phasor, calculated as GP = $(I_{440}-I_{490})/(I_{440}+I_{490})$. Two Gaussian functions were used for fitting every GP histogram.

Days post-confluence	GP_1¶	FWHM ¶	GP_2¶	FWHM¶
1	-0.269 ± 0.037	0.735 ± 0.083	0.325 ± 0.034	0.328 ± 0.050
7	$-0.176 \pm 0.047^{*}$	0.668 ± 0.040	0.380 ± 0.085	0.259 ± 0.026
14	$-0.096 \pm 0.049^{***\blacklozenge}$	0.753 ± 0.123	$0.457 \pm 0.014^{**}$	0.295 ± 0.023

FWHM=Full width at the half maximum.

¶values are presented as mean ± standard deviation.

*p<0.05 to the day 1

**p<0.01 to the day 1

***p<0.001 to the day 1

♦p0.05 to the day 7